Chapter 4 Global Glacial Isostatic Adjustment and Modern Instrumental Records of Relative Sea Level History

W. R. Peltier

4.1 INTRODUCTION

In our effort to understand the implications of the secular variations of relative sea level so clearly recorded on tide gauges from which sufficiently long records are available (see Chapter 3), it is important that we recognize the extraordinary range of physical processes that contribute to such observations. Although it is now understood that the record length must be sufficiently long to allow us to average out the influence of the interannual variability associated with El Niño and other processes, it is not as widely understood that very much longer timescale geological processes may also significantly contaminate such observations. Here the word "contamination" refers to the contribution to the secular rate of change of sea level from any process other than those associated with modern climate drift, whether the latter be of "natural" or "anthropogenic" origin. This chapter focuses on the one specific source of geological timescale contamination that appears to dominate all others from the point of view of its global incidence. This concerns the phenomenon of glacial isostatic adjustment (hereafter GIA), a physical process caused by the intense cycle of glaciation and deglaciation to which the planet has been subjected for the past 900,000 years of the Pleistocene period of Earth history (e.g., see the discussion of the oxygen isotopic ice volume proxy from the ODP677 core in Shackleton *et al.*, 1990). Although other geological processes may also contribute to modern observations of secular rates of sea level change in specific regions, for example, near subduction zones where oceanic lithosphere descends into the mantle and where the descent may be accommodated seismogenically through the occurrence of intense dip–slip earthquakes such as are responsible for the continuing uplift of the coast of the Huon Peninsula of Papua New Guinea, these other processes seem not to be of global import and so will not be considered here.

To set the stage for the discussion to follow, consider the analysis of tide gauge secular sea level trends presented in Fig. 4.1, taken from Peltier and Tushingham (1989). It was first established in this paper that the glacial isostatic adjustment process was a significant global source of "contamination" of such

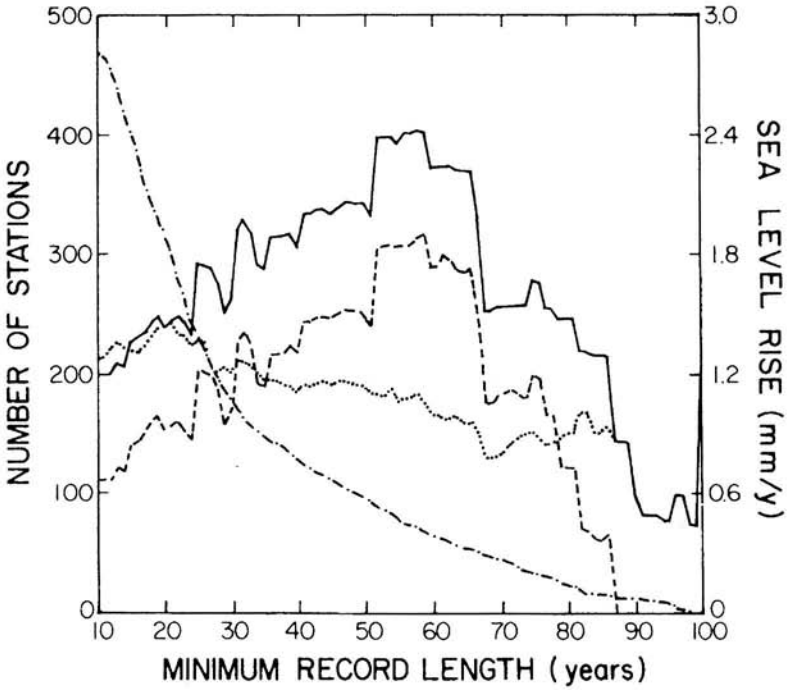

Figure 4.1 Results for the analysis of the global rate of RSL rise obtained from the linear regression analyses of Peltier and Tushingham (1989). The dash-dotted curve depicts the decrease in the number of tide gauge stations as the minimum record length employed in the analysis increases. The three individual estimates of the globally averaged rate of RSL rise versus minimum record length are based upon equal area averages of the raw (dashed curve) and GIA-corrected (solid curve) tide gauge data and a site-by-site average of the corrected data (dotted curve). The solid curve should provide the most accurate linear regression estimate of the present-day global rate of relative sea level rise.

observations. The figure shows (dash–dot line) the way in which the number of tide gauges decreases as a function of the length of the observational record that the individual instruments provide (as of the date of publication of the original paper). The same diagram also shows how the globally averaged rate of secular sea level change varies as a function of the lower timescale cutoff that is applied to determine whether the time series from a given gauge will be allowed to contribute to the determination of the globally averaged rate. The results obtained on the basis of such analyses are shown for two variants of the analysis procedure, one in which the "raw" rates of secular sea level rise are averaged by employing an areal weighting (dashed line) to account for the fact that the tide gauge installations do not sample the ocean surface uniformly, and one in which these areally weighted "raw" rates are "decontaminated" by subtraction of the influence on each gauge that is predicted by a theory of the GIA process (solid curve). In the third of the results (dotted

curve) no attempt to weight the data for area coverage has been made; this is the least meaningful of the three estimates. Two points will be noted by inspection of these results. First, when the tide gauge (areally weighted) rates of secular sea level rise are corrected for the influence of glacial isostatic adjustment, the globally averaged rate of relative sea level (RSL) rise is somewhat increased. Second, and more important, however, is the fact that, as the minimum record length of the set of time series that is employed to determine the average is increased, the globally averaged rate of RSL rise also increases initially. This demonstrates clearly that, when short records are included in the set for which the global average is determined, the short timescale incoherence among them leads to an underestimate of the actual global rate of RSL rise that is ongoing in the Earth system. This point is further illustrated by Fig. 3.11 in the previous chapter of this book.

It is also notable, however, that in the analysis of Peltier and Tushingham (1989) the globally averaged rate determined on the basis of the longest records begins to fall rapidly once the minimum record length exceeds approximately 60 years. This fall is not compatible with the result shown in Fig. 3.11 in the preceding chapter. The reason for this has to do with the fact that in constructing Fig. 4.1 those records which were long but contaminated by local anthropogenic effects (ground water extraction, etc.) were not removed from the mix. To optimize our inference of the ongoing globally averaged rate of relative sea level rise, therefore, we will need to pay close attention to the application of three primary criteria. First, the records we employ must be sufficiently long to enable us to accurately average out the influence of the E1 Niño-related and other interannual variability. Second, we must eliminate all long records known to be strongly contaminated by well-recognized local tectonic or anthropogenic but not climate-related processes. Third, we need to filter these records to remove, as accurately as possible, the contribution to the local rate of secular sea level change at each tide gauge that is due to the influence of GIA.

In what is to follow, I will first review the global theoretical model of the GIA process that my students and I have developed over the past 20 years. Following a brief discussion of the global character of the solutions for the present day rate of RSL rise predicted by this theory, and of the quality of the fits to individual time series in the global data base of Holocene sea level histories that have been achieved with it, I will focus upon the results obtained by employing various versions of the global model to filter the same set of tide gauge data as were employed in Chapter 3 to infer the strength of the global signal that may be related to modern climate change. Finally, I will employ the theory in conjunction with specific observational constraints to show that the contribution to this inferred globally averaged rate of sea level rise that could be ascribed to persistent melting of the Antarctic and Greenland ice sheets since mid-Holocene time is extremely small. These results suffice

to place the onus for the explanation of the observed modern rate of RSL rise squarely upon modern climate change.

4.2 THE MODERN GLOBAL THEORY OF THE GLACIAL ISOSTATIC ADJUSTMENT PROCESS

The theory of the GIA process is embodied in an integral "sea level equation," the solution of which describes the time-dependent separation between the surface of the solid earth and the gravitational equipotential surface that determines the equilibrium level of the sea. This equipotential surface is, of course, precisely the geoid of classical geodesy. The basic ingredients and initial form of this sea level equation (SLE) were developed in Peltier (1974, 1976), Peltier and Andrews (1976), and Farrell and Clark (1976). First solutions were published by Clark *et al.* (1978) and Peltier *et al.* (1978). This rather primitive initial theoretical structure has since been very significantly refined both in regard to the mathematical methods employed to solve the SLE and in regard to the range of physical effects included as influences upon the solution. The most general form of the SLE which governs the time dependence of relative sea level subsequent to the onset of any variation of land ice cover is as follows (see Peltier, 1998a for a most up-to-date review and detailed discussion), with $S(\theta, \lambda, t)$ the variation of relative sea level at latitude θ and longitude λ as a function of time t:

$$S(\theta, \lambda, t) = C(\theta, \lambda, t) \left[\int_{-\infty}^{t} dt' \iint_{\Omega} d\,\Omega' \{ L(\theta', \lambda', t')\, G_{\phi}^{\mathrm{L}}(\gamma, t - t') + \Psi^{\mathrm{R}}(\theta', \lambda', t')\, G_{\phi}^{\mathrm{T}}(\gamma, t - t') \} + \frac{\Delta\Phi(t)}{g} \right]. \tag{1}$$

In Eq. (1) the function $C(\theta, \lambda, t)$ is the so-called "ocean function," which is, by definition, equal to unity where there is ocean and zero elsewhere. This equation is an integral equation because the surface mass load per unit area, L, is composed of both ocean–water and land–ice components. It takes the explicit form

$$L(\theta, \lambda, t) = \rho_{\mathrm{I}}\, I(\theta, \lambda, t) + \rho_{\mathrm{w}}\, S(\theta, \lambda, t) \tag{2}$$

in which $I(\theta, \lambda, t)$ is the space–time history of ice-thickness variations and $S(\theta, \lambda, t)$ is the space–time variation of ocean–water thickness variations. The latter is, of course, simply relative sea level itself. Due to the composite property of L expressed in Eq. (2), the unknown observable function S appears both on the left-hand side of (1) and under the triple convolution operator on the right-hand side of (1). The theory embodied in (1) is thus of integral equation form and may be employed to determine S given an assumed known history of glaciation and deglaciation $I(\theta, \lambda, t)$, together with suitable impulse

response functions (Green functions) G_ϕ^{L} and G_ϕ^{T}. These Green functions embody all of the information concerning the radial viscoelastic structure of the earth that is required to determine the impact of this structure upon relative sea level history. In terms of the surface load and tidal "Love numbers," $(h^{\mathrm{L}}, k^{\mathrm{L}})$ and $(h^{\mathrm{T}}, k^{\mathrm{T}})$, respectively, these Green functions have the following mathematical forms, which consist of infinite series expansions in Legendre polynomials $P_\ell(\cos\,\theta)$ in which ℓ is spherical harmonic degree:

$$G_\phi^{\mathrm{L}}\,(\theta, \lambda, t) = \frac{a}{m_{\mathrm{e}}} \sum_{\ell=\mathrm{o}}^{\infty} (1 + k_\ell^{\mathrm{L}}\,(t) - h_\ell^{\mathrm{L}}\,(t))\, P_\ell\,(\cos\,\theta), \tag{3a}$$

$$G_\phi^{\mathrm{T}}\,(\theta, \lambda, t) = \frac{1}{g} \sum_{\ell=0}^{\infty} (1 + k_\ell^{\mathrm{T}}\,(t) - h_\ell^{\mathrm{T}}\,(t))\, P_\ell\,(\cos\,\theta). \tag{3b}$$

The Love numbers in turn have Dirichlet series expansions of the form (Peltier 1976)

$$h_\ell^{\mathrm{L}}(t) = h_\ell^{\mathrm{E}}\,\delta(t) + \sum_{j=1}^{J} r_j^\ell\, e^{-s_j^\ell t} \tag{4a}$$

$$k_\ell^{\mathrm{L}}(t) = k_\ell^{\mathrm{E}}\,\delta(t) + \sum_{j=1}^{J} q_j^\ell\, e^{-s_j^\ell t}. \tag{4b}$$

In these Dirichet series the $h_\ell^{\mathrm{H,E}}$ and $k_\ell^{\mathrm{H,E}}$ are precisely the elastic surface load Love numbers of Farrell (1972) which measure the magnitude of the response to application of a load that varies as a delta function in time. The quantity $\delta(t)$ is the Dirac delta function, the s_{j}^ℓ are a set of normal mode "poles" in the plane of the complex Laplace transform variable "s" representing the inverse relaxation times of modes of "viscous gravitational relaxation" (Peltier, 1976), and the r_j^ℓ and q_j^ℓ are the residues at these poles that may be determined in the usual way using Cauchy's residue theorem (Peltier, 1985) or the collocation technique described previously in Peltier (1974). The tidal Love number counterparts of $(h_\ell^{\mathrm{L}}, k_\ell^{\mathrm{L}})$, namely $(h_\ell^{\mathrm{T}}, k_\ell^{\mathrm{T}})$, have expansions of precisely the same form as (4a) and (4b) but they are determined subject to the boundary conditions that are appropriate when the responses arise through an imposed variation in the gravitational potential field rather than through an imposed surface mass load (see Farrell, 1972, for details).

Solutions to the sea level equation (1) are constructed using an iterative methodology that is based upon the recognition that the influence of time variations in the ocean function $C(\theta, \lambda, t)$ and the influence of the feedback onto sea level of the changing rotational state of the planet due to the variations of surface mass load described in (1) by the convolution of Ψ^{R} with $\mathrm{G}_\phi^{\mathrm{T}}$ are both second-order effects. The complete algorithm that I have developed to incorporate these effects, as discussed in Peltier (1994, 1998a, 1999), begins with the construction of a solution to (1) which neglects both of these effects

and which is derived using the semispectral algorithm described in Mitrovica and Peltier (1991)—an algorithm that delivers a solution $S(\theta, \lambda, t)$ in terms of the time-dependent coefficients in an expansion of the solution on a basis of spherical harmonics. Solutions are now typically computed at very high spatial resolution by truncating the spherical harmonic expansions to degree and order 512. Given this first approximation to the full solution, we have complete knowledge of the variations of surface mass load associated with the glacial cycle, the component $I(\theta, \lambda, t)$ having been an assumed known input to (1) that may be varied to improve the fit to the observations and the component $S(\theta, \lambda, t)$ being the output from its solution. The surface load $L(\theta, \lambda, t)$ in (2) is thus entirely determined.

In the second step of this iterative process we next compute the rotational response to this history of surface loading by solving the Euler equation,

$$\frac{d}{dt}(J_{ij}\,\omega_j) + \varepsilon_{ijk}\,\omega_j\,J_{k\ell}\,\omega_k = 0, \tag{5}$$

in which J_{ij} is the moment of inertia tensor of the planet, ω_j are the components of its angular velocity vector, and ε_{ijk} is the Levi–Cevita alternating tensor. Assuming a biaxial form for the undeformed shaped of the planet, accurate solutions to (5) may be constructed by employing the standard perturbation expansion

$$\begin{aligned} \omega_i &= \Omega\,(\delta_{ij} + m_i) \\ J_{ij} &= I_{ij}, \qquad i \neq j \\ J_{11} &= A + I_{11} \\ J_{22} &= A + I_{22} \\ J_{33} &= C + I_{33}, \end{aligned} \tag{6}$$

in which (A, A, C) are the principal moments of inertia, Ω is the basic state angular velocity of the earth, and I_{ij} and m_i are (assumed small) fluctuations away from the basic state values. To first order in these fluctuations (Munk and MacDonald, 1960), substitution of (6) into (5) leads to the following decoupled system for polar motion and earth rotation, respectively, as

$$\frac{\mathrm{i}}{\rho_r}\,\dot{\mathbf{m}} + \mathbf{m} = \boldsymbol{\Psi} \tag{7a}$$

$$\dot{m}_3 = \dot{\Psi}_3, \tag{7b}$$

in which the overdot indicates a time derivative, the so-called excitation functions are $\boldsymbol{\Psi}$ and $\dot{\Psi}_3$, $\sigma_r = \Omega\,(C - A)/A$ is the Chandler wobble frequency of the rigid earth, $\mathbf{m} = m_1 + i\,m_2$, $\boldsymbol{\Psi} = \Psi_1 + i\,\Psi_2$, $i = \sqrt{-1}$, and the Ψ_i are

$$\Psi_1 = \frac{I_{13}}{(C - A)} + \frac{\dot{I}_{23}}{\Omega(C - A)}, \tag{8a}$$

$$\Psi_2 = \frac{I_{23}}{(C - A)} - \frac{\dot{I}_{13}}{\Omega(C - A)}, \tag{8b}$$

$$\Psi_3 = -\frac{I_{33}}{C}. \tag{8c}$$

Now the functions I_{ij} and thus the excitation functions Ψ_i are entirely determined by the surface loading history $L(\theta, \lambda, t)$ in Eq. (2), which is known from the first step in the iterative procedure [the details of these relationships are discussed in Peltier (1982) and Wu and Peltier (1984)]. Because the changes in the moments of inertia induced by surface loading also depend upon the redistribution of mass in the interior of the planet that is induced by the surface loading process, and because the redistribution of "internal mass" also depends upon the (assumed radial) viscoelastic structure, the excitation functions also depend upon this structure. Peltier (1982) and Wu and Peltier (1984) show in detail how to employ Laplace transform methods to construct complete solutions to Eqs. (7a) and (7b) for the time dependence of the perturbations to the angular velocity vector of the planet $\omega_i(t)$, $i = 1, 3$. No useful purpose would be served by repeating here the details of the algebraically complex analyses that are required to construct this solution for the rotational response to deglaciation.

In the third step of the iterative procedure we next construct the forcing function Ψ^R in (1) required to compute the impact upon sea level due to this changing rotational state. Because the solution of Peltier (1982) and Wu and Peltier (1984) used to determine the $\omega_i(t)$ is based upon the assumption that $\omega_i/\Omega \ll 1$, this same assumption must be made in computing Ψ^R. Dahlen (1976), in the context of his analysis of a different problem, has shown that the appropriate general solution for Ψ^R, correct to first order in perturbation theory, has the spherical harmonic expansion

$$\Psi^R = \Psi_{00}\, Y_{00}\,(\theta, \lambda) + \sum_{m=-1}^{+1} \Psi_{2m}\, Y_{2m}\,(\theta, \lambda), \tag{9}$$

in which the coefficients Ψ_{ij} are related to the $\omega_i(t)$ by

$$\Psi_{00} = \frac{2}{3}\omega_3(t)\ \Omega a^2 \tag{10a}$$

$$\Psi_{20} = -\frac{1}{3}\omega_3(t)\ \Omega a^2 \sqrt{4/5} \tag{10b}$$

$$\Psi_{2-1} = (\omega_1(t) - i\omega_2(t))\ (\Omega a^2/2)\ \sqrt{2/15} \tag{10c}$$

$$\Psi_{2+1} = (\omega_1(t) + i\omega_2(t))\ (\Omega a^2/2)\ \sqrt{2/15}. \tag{10d}$$

Given Ψ^R we may now complete the third step in the iterative procedure by solving (1) once more for $S(\theta, \lambda, t)$, this time incorporating the influence of the changing rotational state of the planet, the first of the two second-order effects that the iterative procedure is intended to capture.

Now these first three steps in the iterative procedure have been based upon the assumption that the ocean function $C(\theta, \lambda, t)$ was constant and equal to its present-day form. The fourth step in the iterative procedure involves relaxing this assumption and this may be accomplished by following the procedure first described in Peltier (1994), which exploits the fact that the sea level equation (1), being itself a construct of first-order perturbation theory, delivers a solution for relative sea level $S(\theta, \lambda, t)$ that is "relative" to an unspecified and therefore arbitrary datum. This arbitrariness may be exploited to construct what I have previously referred to as a "topographically self-consistent" solution for RSL history. The procedure is simply as follows: First, we define a time-independent field $T'(\theta, \lambda)$ such that when we add it to the solution of the SLE computed for the present day (time $t = t_p$), we obtain the known present-day topography of the planet with respect to sea level, as

$$S(\theta, \lambda, t_p) + T'(\theta, \lambda) = T_p(\theta, \lambda), \tag{11}$$

in which T_p is the present-day topography wrt sea level, determined, say, by the ETOPO5 data set. Using (11) to define $T'(\theta, \lambda)$ we may then determine the topography at any time in the past by computing

$$T(\theta, \lambda, t) = S(\theta, \lambda, t) + [T_p(\theta, \lambda) - S(\theta, \lambda, t_p)]. \tag{12}$$

The true paleotopography, including the contribution from the ice sheets of thickness $I(\theta, \lambda, t)$, is then

$$PT(\theta, \lambda, t) = T(\theta, \lambda, t) + I(\theta, \lambda, t). \tag{13}$$

At any point in space and at any instant of time for which $PT < 0$ we therefore have ocean, whereas "land" is where $PT > 0$ (the only exception to this general rule concerns a number of low-lying inland seas (such as Caspian Sea) whose surfaces clearly do not lie on the same equipotential surface as does the global ocean). Subject to this caveat we may define a first approximation to the actual time-dependent ocean function as

$$\begin{aligned} C^1(\theta, \lambda, t) &= 1 \quad \text{for} \quad PT < 0 \\ C^1(\theta, \lambda, t) &= 0 \quad \text{for} \quad PT > 0. \end{aligned} \tag{14}$$

In reconstructing the topogarphy PT it is also important to recognize the "implicit" component of the ice load (Peltier 1998c) that is activated in the solution of (1) because of the perturbation theory–based nature of this equation. Since the fact that the redefinition of land to sea that occurs (for example) when the initially ice-covered Hudson Bay, Barents and Kara Seas, and the Gulf of Bothnia become connected to the ocean is a nonperturbative effect,

the "explicit" component of the ice load that is varied in (1) to enable the model to fit the data must be considered to be an "effective" load. To compute the actual load and thus the true paleotopography, one must add to the effective load the additional "implicit" component. This completes step 4 of the iterative procedure. The next step in the process involves executing the first four steps in the process a second time, ending with a second guess for the time-dependent ocean function $C^2(\theta, \lambda, t)$ and, of course, with a new solution for relative sea level history $S(\theta, \lambda, t)$ that incorporates the full influence of rotational feedback.

Before discussing the impact of the global process of glacial isostatic adjustment on modern tide gauge–based estimates of secular sea level change, in the next section I will first discuss the global form of the solutions which the above-discussed theory delivers for the present-day rate of relative sea level rise and the extent to which it is able to provide satisfactory fits to a globally distributed set of relative sea level history observations. It will thereafter prove interesting not only to discuss the sea level signature that a specific tide gauge might be expected to measure but also to consider the signature of the time rate of change of absolute sea level (geoid height) that would be observed by an artificial Earth-orbiting satellite, either one equipped with an altimeter to measure distance from the satellite to the sea surface (e.g., TOPEX/POSEIDON; see Chapter 6 for details of the way in which this system has already been employed to address the issue of global sea level change) or one that may be employed to infer this signal through measurement of the time dependence of the space-dependent strength of the gravitational field itself (expressed in terms of the time dependence of geoid height). The latter measurement is one that will be made at very high resolution in the near future using the GRACE satellite, and the CHAMP precursor, as discussed in greater detail in Peltier (1999).

4.3 GLOBAL PROPERTIES OF PRESENT-DAY SIGNATURES OF THE GIA PROCESS: TUNING THE MODEL

Since the solutions of the SLE that are of interest insofar as their predictions of present-day rates of sea level change are concerned are clearly those based upon models of the radial viscoelastic structure of the planet that best reconcile the available data base of geological timescale observations, it is clearly important to first establish that the theory embodied in the SLE does indeed satisfy these long timescale constraints when its physical properties are appropriately selected.

The primary data base used to tune the global model of the GIA process that is embodied in the SLE consists of radiocarbon-dated records of the variation of the level of the sea relative to the deforming surface of the solid earth. In tuning the properties of the global model to best fit these data, the

elastic properties of the model of the planetary interior, namely, the density ρ and the two elastic Lamé parameters λ and μ, are assumed to be fixed, insofar as their variation with radius is concerned, by the results of free oscillation and body wave propagation seismology. I continue to base my analyses on an elastic structure defined by the PREM model of Dziewonski and Anderson (1981). Since the complete rheology of the interior is assumed to be adequately represented by a linear Maxwell solid, it is described by the Laplace transform domain stress-strain relation (see Peltier (1974) for discussion)

$$\tau_{ij}(s) = \lambda(s)\, e_{ij}(s)\, \delta_{ij} + 2\mu(s)\, e_{ij}(s), \tag{15}$$

in which s is the Laplace transform variable, τ_{ij} is the stress tensor, and e_{ij} is the strain tensor. The compliances $\lambda(s)$ and $\mu(s)$ of the linear Maxwell model are just

$$\lambda(s) = \frac{\lambda s + \mu\kappa/\nu}{s + \mu/\nu}, \tag{16a}$$

$$\mu(s) = \frac{\mu s}{s + \mu/\nu}. \tag{16b}$$

Since the bulk modulus $\kappa = \lambda + 2\mu/3 = \lambda(s) + 2\mu(s)/3$ is independent of s for this rheology, the model clearly has no bulk dissipation. The quantity $T_M = \nu/\mu$ is called the "Maxwell time" and this is the timescale that must be exceeded in order to effect the transition from Hookean elastic to Newtonian viscous behavior in response to an applied shear stress that is embodied in the Maxwell model. With (ρ, λ, μ) fixed by seismology, the only free parameter in the model is therefore the molecular viscosity ν. For the purpose of all of the analyses herein, the model of the interior of the earth is assumed to be spherically symmetric both in elasticity and in viscosity. It is this basic assumption that leads to the simple mathematical expressions (3a) and (3b) for the Green functions G_ϕ^L and G_ϕ^T. Since $\rho(r)$, $\mu(r)$, and $\lambda(r)$ of this spherically symmetric model are very well constrained seismologically (as defined by PREM), we are at liberty to vary only $\nu(r)$ in order to tune the model to fit the geological timescale observations. Given that the effective creep resistance of a solid (its viscosity) is strongly temperature dependent because the creep resistance of a solid is thermally activated, and because the mantle of the earth is assumed to be undergoing a process of thermally forced convection in which lateral variations of temperature are expected to be intense, it is clear that mantle viscosity must be a function of all three space coordinates. By employing a spherically symmetric model of the GIA process, we will therefore be testing the hypothesis that the aspherical viscosity structure that must characterize the actual mantle of the earth has no unambiguously observable effect. This is expected to be the case only if the actual lateral variations occur on sufficiently small horizontal scale, say over distances only on the order

of the thickness of the lithosphere. As we will show immediately, spherically symmetric models of the internal structure can reconcile most of the available geological observations exceptionally well. There are, of course, exceptions to this general rule in the form of relative sea level observations from sites undergoing active tectonic uplift or subsidence, but these appear to constitute local exceptions to the general rule that the best fitting spherically symmetric model is able to reconcile the vast majority of the observations very well.

A sequence of three viscosity models for which I will explicitly discuss RSL predictions herein is illustrated in Fig. 4.2, where the models are labeled VM1, VM2, VM3 with the letters VM simply representing "viscosity model" and the number affixed following the letters being employed to distinguish the models from one another. Given a viscosity model and a model $I(\theta, \lambda, t)$ of the process of glaciation and deglaciation, we have all that is required to fix the inputs to Eq. (1) and thus to make predictions of postglacial relative sea level history. For all of the analyses discussed in this chapter, I will assume that the ICE-4G model described in Peltier (1994, 1996) adequately describes the last deglaciation even of the current ice age. Northern Hemisphere isopacks from this model for six different instants of time are shown in Fig. 4.3 (see color plate). It is important to understand that, although it is expected that this model is close in form to the actual deglaciation event that began approximately 21,000 calendar years ago, it cannot be exact and is still being refined in the course of work to develop an improved ICE-5G follow-on model.

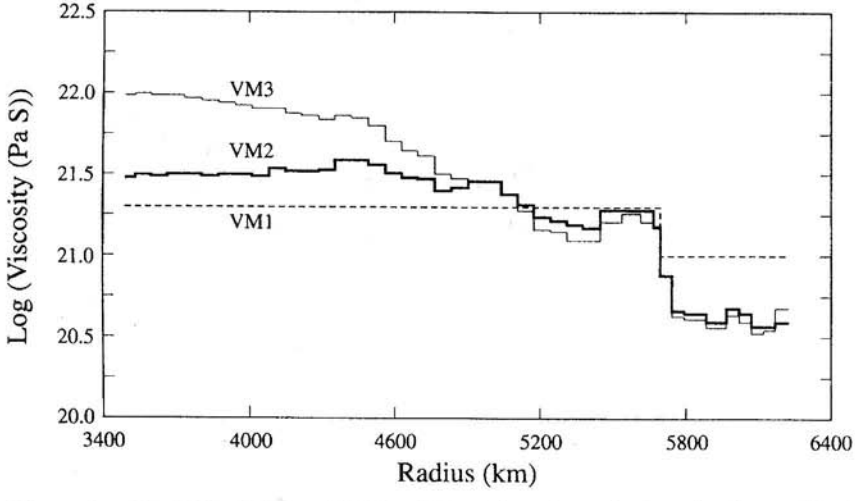

Figure 4.2 The VM1, VM2, and VM3 radial profiles of mantle viscosity discussed in the text. These represent the range of smooth viscosity profiles that have been employed for this physical property of the spherically symmetric viscoelastic models of the glacial isostatic adjustment process.

Figures 4.4 and 4.5 (see color plates) display comparisons of the present-day predicted rate of relative sea level rise as a function of the viscosity model (Fig. 4.4 shows the predictions of VM1 and VM2 together with their difference) and as a function of whether the influence of rotational feedback is included in the analysis (Fig. 4.5 presents results for viscosity model VM2 both including and excluding the rotational feedback effect as well as the difference between these two predictions). Inspection of these two figures will reveal all of the salient geographical characteristics of the global GIA process. Figure 4.4, for example, demonstrates that the regions that were ice-covered at LGM (Last Glacial Maximum) are regions in which relative sea level is currently falling as a consequence of ongoing postglacial rebound of the crust of the solid earth. Likewise, in the regions peripheral to those that were glaciated, relative sea level is predicted to be rising at present due to the collapse of the "glacial forebulge." The latter feature is a pronounced characteristic of the glaciated state and is a region in which the local radius of the planet is increased because of the mass that has been extruded from under the ice-loaded region as the earth isostatically adjusts to the weight of the surface load. When the ice load is removed and the rebound of the crust in the loaded region commences, the peripheral bulge of the solid earth begins to collapse. Beyond the region of forebulge collapse, in what I have previously referred to as the "far field" of the ice sheets, the rate of RSL change signal is characterized by a slow fall of RSL in ocean basin interiors and a region of similarly weak sea level rise confined to a "halo" around the coastline of each of the far field continents. The nature of the pattern of RSL rise/fall in the far field of the ice sheets may be understood as arising from the fact that, as the earth's shape relaxes following deglaciation, water is continuously "siphoned" from the central ocean basins in order to fill the depressions that are being created by proglacial forebulge collapse and by the "hydroisostatic tilting" of far field continental coastlines due to the weight applied to the surface by the offshore water load. Comparing the predictions of the VM1 and VM2 viscosity models demonstrates that the region in which the difference between them is largest is along the U.S. east coast. This region is therefore the one in which one would first look to discriminate between them.

Before discussing explicit analyses of this kind, it will be instructive to consider the similar set of predictions shown in Fig. 4.5, which has been designed to illustrate the impact of rotational feedback on the GIA-induced sea level signal. Results are shown in this figure for the VM2 model with and without this feedback included. The difference between the two predictions in the lower part of this figure shows that the influence of rotational feedback is very modest indeed, insofar as the amplitude of this signal is concerned. Furthermore, the pattern of the difference is almost entirely that of a degree 2 and order 1 Legendre polynomial, indicating on the basis of Eq. (10) that it is the polar wander component of the rotational response to GIA that feeds back most strongly onto sea level. It is important to note that the extremely

weak influence of rotational feedback is at extreme odds with the contrary suggestion by Bills and James (1996), whose incorrect analysis of this problem led them to the conclusion that the strength of the rotational feedback was 1–2 orders of magnitude larger.

By way of demonstrating the way in which ^{14}C-dated RSL histories may be employed to discriminate between competing models of the radial viscosity structure, Fig. 4.6 shows an intercomparison of predictions of ICE-4G (VM1) and ICE-4G (VM2) for a sequence of 16 locations along the east coast of the continental United States at which ^{14}C-dated RSL histories are available. Also shown in this figure are RSL predictions for this set of locations for a model of Mitrovica and Forte (1997) which differs most extremely from both VM1 and VM2 in that it has a transition zone between 400 and 660 km depth in which the viscosity is extremely low (a feature that is balanced by the existence of a high-viscosity region in the middle of the lower mantle; see Peltier (1998a) for a figure explicitly comparing this model with VM2). Inspection of the results in Fig. 4.6 shows that the Mitrovica and Forte model is entirely excluded by the data because its "channel flow" characteristics predict the existence of raised beaches to the immediate south of the ice margin that are not observed. Channel flow models of this kind, in which the viscous flow of mantle material is confined to a low-viscosity near-surface region, have been known to be excluded by U.S. East coast RSL observations after the analyses presented by Cathles (1975) and Peltier (1974). Comparing the predictions of ICE-4G (VM1) and ICE-4G (VM2) demonstrates that at all sites along the northernmost part of the U.S. east coast the VM1-based model drastically overpredicts the present-day rate of RSL rise whereas the VM2 based model essentially eliminates these misfits.

As discussed most recently in Peltier (1998b), the viscosity model VM2 was in fact deduced on the basis of the application of the formal theory of Bayesian inference to a small subset of GIA data. In this procedure, model VM1 was employed as a starting model and the Fréchet kernels for the observed data were used to refine this model to optimally reduce the misfits of the starting model to the observations. None of the U.S. east coast data were employed in this process; rather they were withheld to provide a definitive check on the improvement to the model delivered by the automated inversion procedure. The data used for inversion actually consisted of the set of wavenumber-dependent relaxation times inferred by McConnell (1968) to characterize the postglacial recovery of Fennoscandia (the validity of which was recently reconfirmed by Weiczerkowski *et al.*, 1999), a set of approximately 23 relaxation times inferred on the basis of exponential fits to ^{14}C-dated RSL curves from both Canada and Fennoscandia, and the observed rate of nontidal acceleration of planetary rotation. VM2 serves as a good zeroth-order model of the radial variation of viscosity based upon numerous posteriori tests of its predictions against the very large set of observations that were not employed in its construction (see Peltier 1998a). Given this zeroth-order acceptable

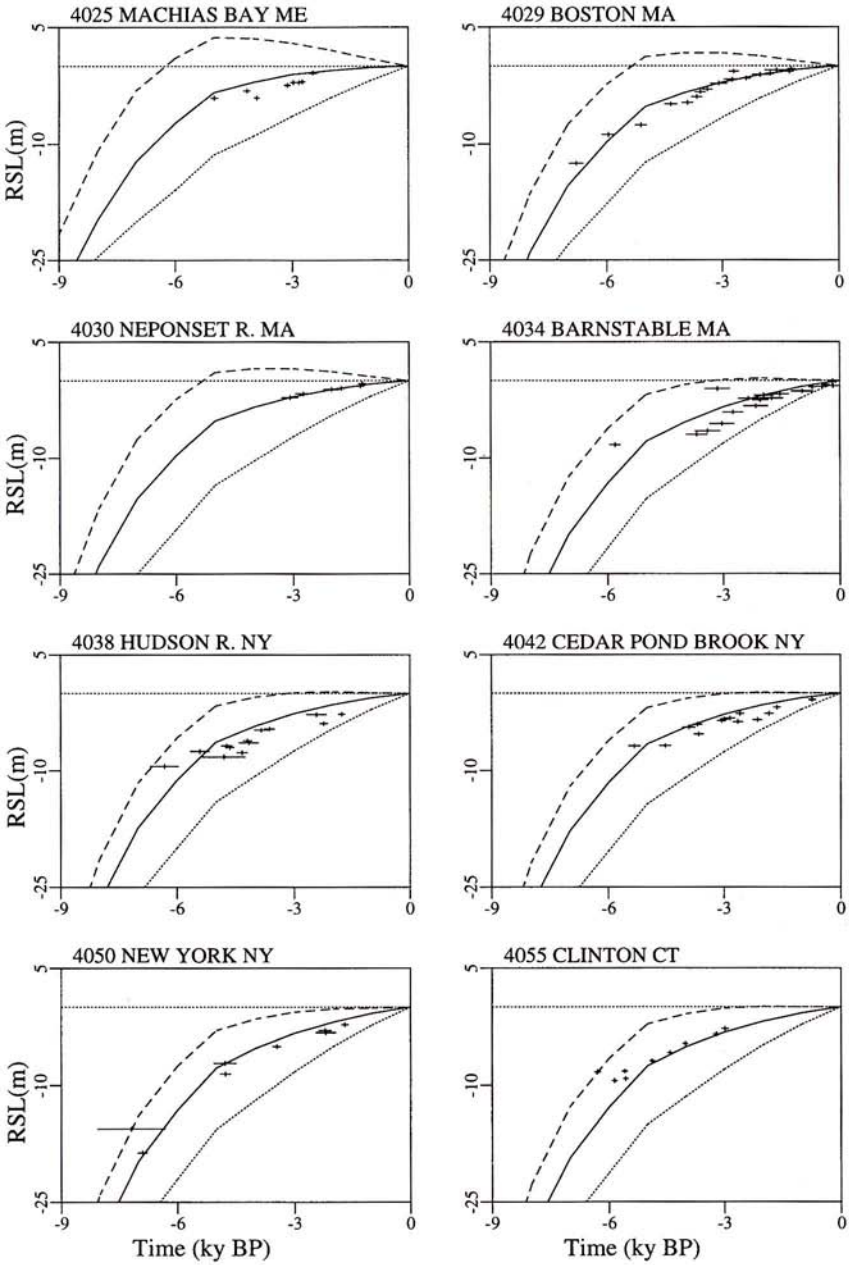

Figure 4.6 Predicted histories of relative sea level change at 16 sites along the eastern coast of the North American continent based upon use of the ICE-4G model of the deglaciation history. Results are shown for three different models of the radial variation of viscosity, respectively VM1 (dotted lines) and VM2 (solid lines) and a third model MF (dashed lines) recently obtained by Mitrovica and Forte (1997) by the simultaneous inversion of both glacial isostatic adjustment and aspherical geoid constraints. It will be clear that model MV2 entirely eliminates the misfits

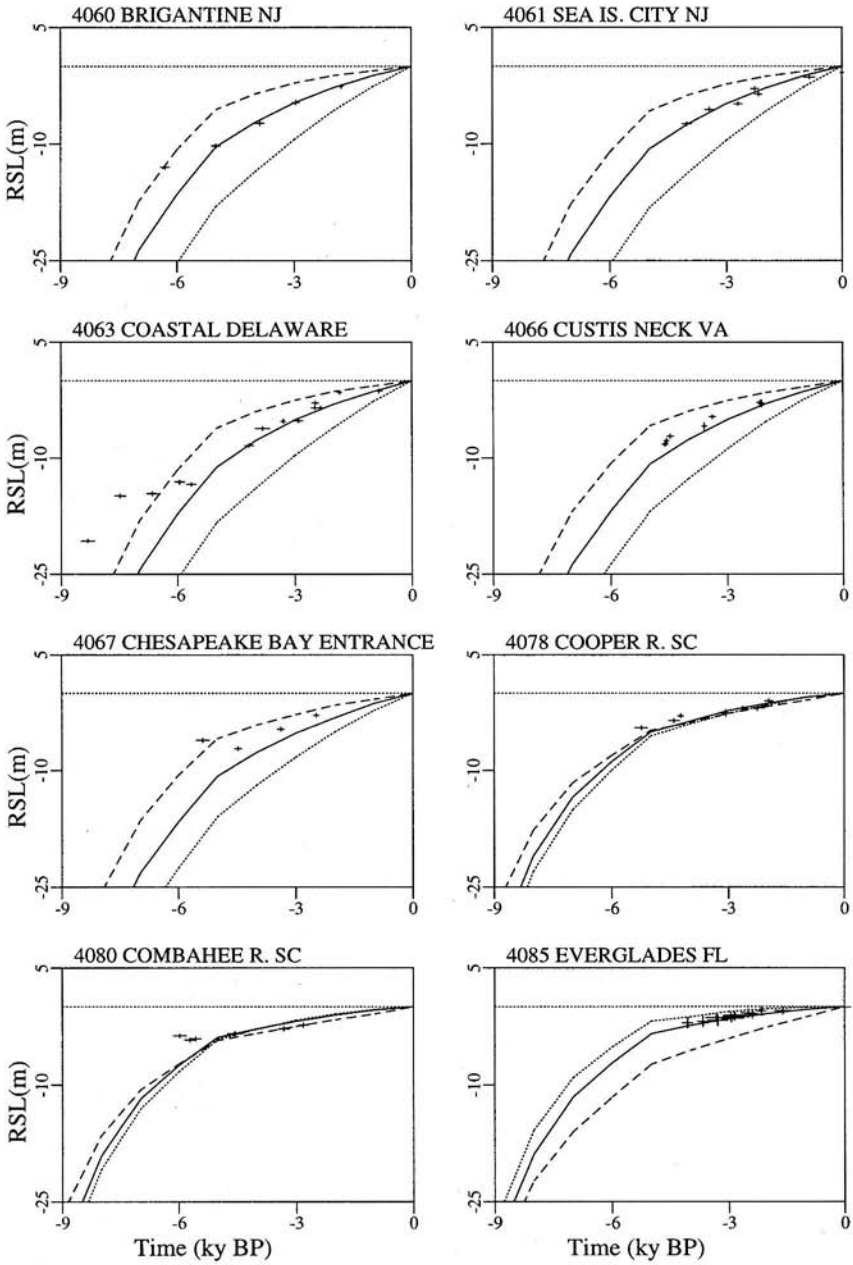

of model VM1 to these data (which were not employed to constrain VM2) and that model MF grossly misfits the observations at essentially all locations along this coast. As discussed in Peltier (1998a), model MF is a "channel flow" model in which the upper mantle and transition zone have such low viscosity that adjustment takes places through motions that are essentially confined to this region. Models of this kind have been known not to fit the GIA constraints since the earliest work of Cathles (1975) and Peltier (1974).

model for the global GIA process, we will proceed in the following section to examine the extent to which the GIA process is expected to contaminate tide gauge observations of secular sea level trends.

Before we pursue this line of argument, however, it will prove interesting to consider the nature of the global sea level signal that an artificial earth satellite designed to measure the time dependence of Earth's gravitational field might be expected to observe. Since this signal will be measured relative to the center of mass of the planet rather than relative to the surface of the solid earth, it will be clear that it need look nothing at all like the fields shown on Figs. 4.4 or 4.5. If we denote by $\dot{RSL}$ (θ, λ, t) the rate of relative sea level change with respect to the surface of the solid earth, and by $\dot{RAD}$ (θ, λ, t) the rate of change of the local radius of the planet measured with respect to the center of mass, then it will be clear that $\dot{ABS}$ (θ, λ, t), the rate of change of absolute sea level measured with respect to the center of mass, is just

$$\dot{ABS}\ (\theta, \lambda, t) = \dot{RSL}\ (\theta, \lambda, t) + \dot{RAD}\ (\theta, \lambda, t). \tag{17}$$

Figures 4.7 and 4.8 (see color plates) show both of the component parts of $\dot{ABS}$ together with $\dot{ABS}$ itself for models which respectively exclude (Fig. 4.7) and include (Fig. 4.8) the influence of rotational feedback, both of which employ the ICE-4G (VM2) model as input. Figure 4.9 (see color plate) shows the predictions with and without rotational feedback together with the difference between the predictions. The difference is clearly identical to the degree 2 and order 1 pattern shown previously in Fig. 4.5 as must, of course, be the case.

These results for absolute sea level, which constitute predictions of what the GRACE and CHAMP satellites should see if the GIA process were the only process currently influencing large-scale absolute sea level (geoid height) variability in the Earth System (see Peltier, 1999, for further discussion), demonstrate that the impact of rotational feedback on this observation will not be negligible even though it is negligible insofar as its impact upon sea level history relative to the surface of the solid earth is concerned. It will be extremely exciting over the next decade to keep careful watch on the outcomes of these ultra-high-resolution satellite experiments. They promise to provide a wealth of new knowledge concerning Earth system form and process. One useful prediction which we can make at present, however, by averaging the $\dot{ABS}$ signals shown in Figs. 4.7 and 4.8 over the area of the oceans covered by TOPEX/POSEIDON, is that the global rate of RSL rise estimated on the basis of this measurement system must be corrected upward by approximately 0.30 mm/yr in order to correct for the ongoing influence of the glacial isostatic adjustment process. This is a significant upward revision of the number of 0.08 mm/yr previously cited in Peltier (1998) in reference to a first attempt by Rapp *et al.* (personal communication) to compute the magni-

tude of the GIA contamination based upon the ICE-4G (VM2) model predictions.

4.4 GIA-DECONTAMINATED TIDE GAUGE ESTIMATES OF THE RATE OF GLOBAL SEA LEVEL RISE

For the purpose of producing the best tide gauge–based estimate of the global rate of relative sea level rise which is not contaminated by the influence of the glacial isostatic adjustment process, I will focus first upon the results obtained by applying the highest resolution version of the ICE-4G (VM2) model for which results have been computed. These results are presented in Table 4.1 in which analyses are shown for 27 tide gauges, each of which is characterized by more than 70 years of observations. As discussed in detail by Douglas (1991), and as demonstrated by the earlier results of Peltier and Tushingham (1989) shown previously in Fig. 4.1, it is extremely important for the stability of the global estimate that one employ only very long records in such analyses since the interannual variability of relative sea level is intense and must be effectively averaged out if an accurate estimate is to be obtained. In Table 4.1 the individual columns give the latitude and longitude locations of each of the gauges, the number of years in the record and the estimate by Douglas ("Doug.") (Chapter 3) for the rate of relative sea level rise determined on the basis of a best fitting linear model to the raw annually averaged tide gauge data. Five columns of additional information labeled with the numbers -0.5, 0.5, 1.5, 2.5, 3.5 list the difference between the observed rates of RSL rise of Douglas and the GIA predictions for the ICE-4G (VM2) model of the rate of RSL rise that is predicted to occur at each of the tide gauge sites and at each of the times before present (measured in 1000 years) represented by the numbers -0.5 to $+3.5$, if the only process acting in the Earth System were the global process of glacial isostatic adjustment. The column labeled LSQ presents the difference between the Douglas calculation and the rate of relative sea level rise associated with the GIA process at each gauge determined by a linear least-squares fit to the theoretical predictions over the age range from 3.5 kyr before present to 0.5 kyr in the future. By including the LSQ result in our analysis, we will be able to estimate the magnitude of the error that would be committed by using the ^{14}C-dated geological data in the way employed by Gornitz (1995) in her analysis of U.S. east coast data. She obtained an estimate of the regional rate of RSL rise based upon GIA decontaminated tide gauge data from this coast of 1.5 mm/yr, a number that is significantly lower than that later obtained by Peltier (1996b), whose analysis of the data from the same region gave an average value near 1.9 mm/yr. At the bottom of the table is listed the average rate of RSL rise determined by simply averaging the observations of Douglas together with a standard deviation of the individual observations from this average value. For each of the

Table 4.1

Rates of Sea Level Rise, Adjusted from Tide Gauge Data

Station	LAT	LON	YRS	Doug. (mm/yr)	Diffs [Douglas–Peltier] (mm/yr)					
					LSQ	−0.50	0.50	1.50	2.50	3.50
Lagos	37.10	−8.40	83	1.40	1.66	1.73	1.67	1.65	1.66	1.68
San Diego (Quara)	32.40	−117.00	74	1.90	1.78	1.98	1.85	1.76	1.71	1.68
Pensacola	30.20	−87.00	73	2.10	1.60	1.84	1.76	1.59	1.48	1.37
Fernandina	30.40	−81.30	96	2.00	1.38	1.60	1.59	1.38	1.25	1.07
Boston	42.20	−71.00	76	2.70	1.91	2.37	2.22	1.95	1.69	1.27
Halifax	44.40	−63.40	76	3.40	1.86	2.58	2.29	1.97	1.53	0.96
Aberdeen I & II	57.15	−2.08	97	0.70	1.20	1.18	1.12	1.19	1.24	1.33
Newlyn	50.10	−5.55	82	1.70	1.15	1.51	1.33	1.18	0.99	0.81
Brest	48.38	−4.50	91	1.30	0.73	1.10	0.92	0.76	0.57	0.37
Cascais	38.68	−9.42	88	1.60	1.84	1.91	1.84	1.82	1.84	1.86
Marseille	43.30	5.35	96	1.20	1.26	1.36	1.30	1.24	1.23	1.23
Genoa	44.40	8.90	92	1.20	1.30	1.38	1.32	1.29	1.28	1.30
Trieste	45.65	13.75	92	1.10	1.17	1.27	1.23	1.15	1.12	1.12
Auckland	−36.87	174.80	85	1.30	1.58	1.84	1.65	1.53	1.53	1.54
Dunedin	−45.88	170.50	89	1.40	1.79	1.93	2.00	1.68	1.67	1.68
Lyttelton	−43.60	172.72	85	2.30	2.68	2.88	2.70	2.65	2.65	2.68
Wellington	−41.28	174.78	87	1.70	2.10	2.33	2.16	2.06	2.04	2.06
Honolulu	21.32	−157.87	92	1.50	1.99	1.97	2.18	1.79	1.91	2.12
San Francisco	37.80	−122.47	80	1.80	1.52	1.50	1.63	1.52	1.44	1.35
Balboa	8.97	−79.57	72	1.50	1.74	1.80	1.74	1.68	1.73	1.83
Buenos Aires	−34.60	−58.37	75	1.10	1.59	2.17	1.98	1.35	1.36	1.41
Key West	24.55	−81.80	84	2.20	1.68	1.91	1.87	1.69	1.55	1.38
Charleston I	32.78	−79.93	75	3.30	2.47	2.86	2.74	2.51	2.33	1.85
Baltimore	39.27	−76.58	94	3.10	1.79	2.31	2.18	1.87	1.51	1.00
Atlantic City	39.35	−74.42	85	3.10	1.41	1.89	1.83	1.52	1.09	0.52
New York	40.70	−74.02	97	3.00	1.77	2.33	2.16	1.84	1.50	0.98
Portland	43.67	−70.25	85	1.90	1.83	2.07	2.02	1.85	1.70	1.46
	Average			1.91	1.66	1.91	1.83	1.65	1.54	1.40
	Standard deviation			0.75	0.40	0.47	0.45	0.41	0.41	0.50

five individual times for which the theoretical rates have been computed are listed the average differences between the Douglas observations and the GIA predictions together with a standard deviation. Also shown is the average difference between the observations and the LSQ estimate deduced by least-squares best fit of a straight line to the theoretical predictions over the age range from −3.5 kyr BP to +0.5 kyr in the future.

Careful inspection of the data presented in Table 4.1 indicates that there is no significant difference between the magnitude of the estimate of the globally averaged rate obtained by direct averaging of Douglas observations (this gives 1.91 mm/yr) and the result 1.87 mm/yr determined by averaging the GIA-corrected observations using the GIA prediction for the present day (by averaging the results for +0.5 and −0.5 kyr BP). There is, however, an extremely significant impact achieved by properly correcting the raw tide gauge data for the influence of GIA. Note that the standard deviation of the raw observations of Douglas from the average value is 0.75 mm/yr, whereas the standard deviation of the GIA-corrected rates from their average value is reduced to 0.45 mm/yr. It is therefore abundantly clear that when the tide gauge data are corrected for the GIA influence, the result is an estimate for the global rate of RSL rise that is much less variable as a function of position on Earth's surface. Also of considerable interest in this table is the difference between the globally averaged rates of relative sea level rise (a) determined by the GIA-corrected tide gauge data that are obtained when the GIA rates are accurate estimates for the present epoch and (b) those obtained when the GIA rate is taken to be represented by an average over the most recent 4 kyr of geological history. In the former case the globally averaged rate is 1.87 mm/yr, whereas in the latter case it is 1.66 mm/yr. The impact of employing the latter methodology of Gornitz (1995) is therefore severe, even when viewed from a global perspective. It inevitably leads to an underestimate of the average rate of RSL rise that could be associated with ongoing climate change in the Earth system. However, when viewed locally, as at the locations along the eastern seaboard of the continental United States, the impact of employing methodology (b) is further increased. On consideration of the results listed in Table 4.1 for the Key West, Charleston I, Baltimore, Atlantic City, and New York locations, application of method (b) for making the GIA correction, based upon the direct use of ^{14}C-controlled geological data averaged over the past 4 kyr to determine a rate, will reduce the strength of the inferred climate related contribution by amounts of 0.2, 0.32, 0.45, 0.44, 0.45 mm/yr for these five locations. The average value of the underestimate of the climate-related rate of RSL rise that is made by employing the Gornitz procedure at these five locations is therefore 0.37 mm/yr, which is essentially identical to the difference between the 1.5 mm/yr estimate of Gornitz (1995) and the 1.9 mm/yr estimate of Peltier (1996b) for the U.S. east coast region when the geological data are employed directly to decontaminate the observations. One must accurately estimate the GIA rate appropriate to the present

day in order to accurately effect a decontamination of the tide gauge observations.

Several further consequential issues must be addressed before being satisfied that we have determined the best possible estimate of the global rate of RSL rise that could be associated with modern climate change. The first of these concerns the issue of the geographical representativeness of the raw average data presented in Table 4.1. There are clearly several regions of the Earth's surface that are oversampled by the analysis procedure employed in constructing Table 4.1. Specifically the east coast of North America is highly oversampled, there being six sites from the northern part of this coast (Baltimore, Atlantic City, New York, Boston, Portland, Halifax) and four from the southern part (Pensacola, Key West, Fernandina, Charleston I). Therefore 10 of the 27 gauges employed to produce a "global" estimate of the rate of RSL rise are actually located along one coast of the North Atlantic Ocean. To correct for this over sampling effect we choose to cluster the tide gauge sites as in Table 4.2 in order first to produce an average for each of the individual clusters and then to produce our estimate of the global rate of RSL rise by analyzing the average over these clusters. Inspection of the partition documented in Table 4.2 reveals the tide gauges have been amalgamated into 11 clusters, one of which consists of the data from Aberdeen I and II, both in Scotland and thus from a region that was heavily glaciated at Last Glacial Maximum. We will eliminate these data from further analysis for this reason. At the bottom of Table 4.2 we list the new globally averaged rate of RSL rise that is obtained by averaging over the individual cluster averages of the raw rates, which gives 1.71 mm/yr, and by averaging over the GIA-corrected cluster averages, which gives a value of 1.84 mm/yr. Of equal importance as the fact that the average rate is now somewhat increased when the GIA correction is made is the fact that the standard deviation of the individual cluster averages is reduced from 0.55 to 0.35 mm/yr. If we recall that the equivalent standard deviations for the unclustered data were 0.75 and 0.45 mm/yr, it will be clear that recognition of the oversampling problem has enabled us to further refine our estimate of the global rate of RSL rise that could be related to ongoing climate change in the Earth system.

We still need to understand the meaning of our best estimate, 1.84 mm/yr, of this average. What relative weight should be attached to the individual cluster averages in Table 4.2, considering the different fractional areas of Earth's surface that the individual clusters should represent? Because it would be arbitrary to assign a degree of importance to each of the clusters, I will leave this question as a caveat on the results that have been presented. It is worth noting, however, that the Northwestern European cluster represented by the tide gauges at Newlyn and Brest delivers results that are somewhat lower than those of most of the other clusters when the GIA correction is applied. This need not be taken to imply a problem with the analysis since there is no reason to believe that the influence of modern climate change

Table 4.2

Clustered Rates of Sea Level Rise, Adjusted from Tide Gauge Data

Station	LAT	LON	YRS	Doug. (mm/yr)	Diffs [Douglas–Peltier] (mm/yr) (Time = 0.00)
Aberdeen I & II	57.15	−2.08	97	0.70	1.15
1 location	Av rate of RSL rise, std dev = 0.70, 0.00; Av diff, std dev = 1.15, 0.00				
Newlyn	55.10	−5.55	82	1.70	1.42
Brest	48.38	−4.50	91	1.30	1.01
2 locations	Av rate of RSL rise, std dev = 1.50, 0.28; Av diff, std dev = 1.21, 0.29				
Cascais	38.68	−9.42	88	1.60	1.88
Lagos	37.10	−8.40	83	1.40	1.70
2 locations	Av rate of RSL rise, std dev = 1.50, 0.14; Av diff, std dev = 1.79, 0.12				
Marseille	43.30	5.35	96	1.20	1.33
Genova	44.40	8.90	92	1.20	1.35
Trieste	45.65	13.75	92	1.20	1.25
3 locations	Av rate of RSL rise, std dev = 1.17, 0.06; Av diff, std dev = 1.31, 0.05				
Auckland	−36.87	174.80	85	1.30	1.74
Dunedin	−45.88	170.50	89	1.40	1.97
Lyttelton	−43.60	172.72	85	2.30	2.79
Wellington	−41.28	174.78	87	1.70	2.24
4 locations	Av rate of RSL rise, std dev = 1.67, 0.45; Av diff, std dev = 2.19, 0.45				
Honolulu	21.32	−157.87	92	1.50	2.07
1 location	Av rate of RSL rise, std dev = 1.50, 0.00; Av diff, std dev = 2.07, 0.00				
San Francisco	37.80	−122.47	80	1.80	1.56
San Diego (Quara)	32.40	−117.10	74	1.90	1.91
2 locations	Av rate of RSL rise, std dev = 1.85, 0.07; Av diff, std dev = 1.74, 0.24				
Balboa	8.97	−79.57	72	1.50	1.77
1 location	Av rate of RSL rise, std dev = 1.50, 0.00; Av diff, std dev = 1.77, 0.00				
Buenos Aires	−34.60	−58.37	75	1.10	2.08
1 location	Av rate of RSL rise, std dev = 1.10, 0.00; Av diff, std dev = 2.08, 0.00				
Pensacola	30.20	−87.10	73	2.10	1.80
Key West	24.55	−81.80	84	2.20	1.89
Fernandina	30.40	−81.30	96	2.00	1.59
Charleston I	32.78	−79.93	75	3.30	2.80
4 locations	Av rate of RSL rise, std dev = 2.40, 0.61; Av diff, std dev = 2.02, 0.53				
Baltimore	39.27	−76.58	94	3.10	2.25
Atlantic City	39.35	−74.42	85	3.10	1.86
New York	40.70	−74.02	97	3.00	2.24
Boston	42.20	−71.00	76	2.70	2.29
Portland	43.67	−70.25	85	1.90	2.04
Halifax	44.40	−63.40	76	3.40	2.43
6 locations	Av rate of RSL rise, std dev = 2.87, 0.52; Av diff, std dev = 2.19, 0.20				
	Average of group values				
	RSL rate from tide gauge records, std dev = 1.71, 0.55				
	RSL rate corrected for GIA, std dev = 1.84, 0.35				

should cause sea level to rise at the same rate everywhere, especially if the global rise of level is caused to significant degree by the thermal expansion of the oceans as appears to be the case.

It will be noted on the basis of the data presented in both Tables 4.1 and 4.2 that the sign of the rate of RSL rise that is predicted to be occurring at all locations in the far field of the Pleistocene ice sheets is negative at all of the tide gauge locations from which long time series of data are available. Clearly when the individual tide gauge rates of RSL rise from this region are corrected by removing the GIA contamination, the result is an increase in the rate inferred to be due to ongoing climate change. As it happens the existence of this far field signature of the GIA process may be invoked to place strong constraints on the possible sources of the global rate of RSL rise that is presently occurring in the Earth system. The penultimate section of this chapter will address this interesting but insufficiently appreciated line of argument.

4.5 IMPLICATIONS OF THE MID-HOLOCENE HIGHSTAND OF SEA LEVEL AT SITES DISTANT FROM THE MAIN CONCENTRATIONS OF LGM LAND ICE

Figure 4.10 shows a location map for a large number of equatorial Pacific island locations from which relative sea level information is available for the Holocene epoch of Earth history. Figure 4.11 presents comparisons of the predictions of the same ICE-4G (VM2) model of the relative sea level history that should be observed at each of these island locations (shown as the solid line) together with the data available from each site as recently quality ensured in the paper of Grossman *et al.* (1998). From most of these oceanic islands there is usually only a single high-quality sea level datum available, often consisting of a ^{14}C-dated "notch" cut in coral that is currently observed to be located above local MSL. On each frame of this figure is also shown the predictions for two modifications of the Northern Hemisphere–constrained ICE-4G (VM2) model as well as for this base model itself. These modifications consist of adding to ICE-4G a continuous "melting tail" that continues to add meltwater to the oceans following the time at which the deglaciation event is assumed to have ended in ICE-4G, namely at 4 kyr BP. For the first of these modifications to the ICE-4G model, for which results are shown by the dotted lines on Fig. 4.11, the rate of eustatic sea level rise associated with late Holocene melting has been assumed to be equal to 0.25 mm/yr and all melting is assumed to derive from the Antarctic ice sheet. The second modification to ICE-4G, RSL results for which are shown as the dashed lines on Fig. 4.11, consists of a continuing eustatic sea level rise of strength 0.5 mm/yr, also assumed to be due to ongoing Antarctic melting.

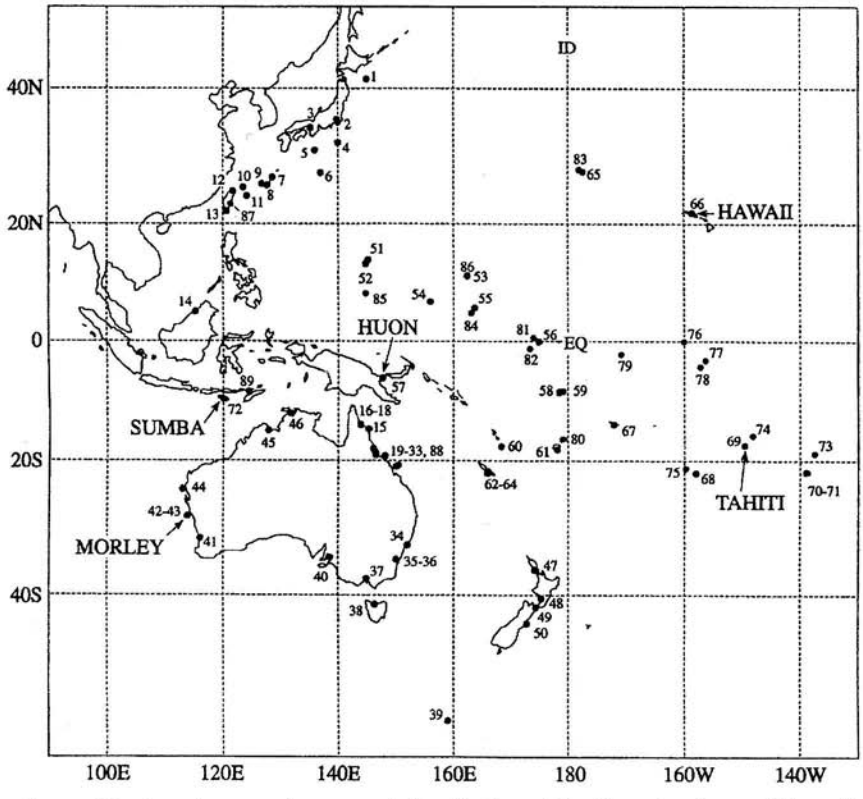

Figure 4.10 Location maps for equatorial Pacific Ocean island locations from which quality-controlled RSL constraints are available in the collection of Grossman *et al.* (1998) which overlaps the earlier compilation of Tushingham and Peltier (1992).

Inspection of the intercomparison of observations and theory shown in Fig. 4.11 demonstrates immediately that the strength of any late Holocene meltwater addition to the global oceans due to sustained melting of the Greenland ice sheet is strongly constrained by the elevation of the mid-Holocene highstand of sea level that is observed at essentially all islands in the equatorial Pacific Ocean from which actual shoreline elevation observations are available. This constraint is sufficiently tight that even continuous melting at the modest rate of 0.25 mm/yr leads to such a sharp reduction in the theoretically predicted amplitude of the highstand, to approximately 1 m rather than the observed 2 m, that it is ruled out by the observations. This same conclusion follows when the continuing melting of polar ice is assumed to derive from Greenland rather than from Antarctica (results not shown). With a rate of late Holocene melting of 0.5 mm/yr, the observed mid-Holocene highstand is entirely eliminated at all locations, as will be clear by inspection of Fig. 4.11. On this basis it would seem that the recent claim by Flemming *et al.* (1998) to the effect

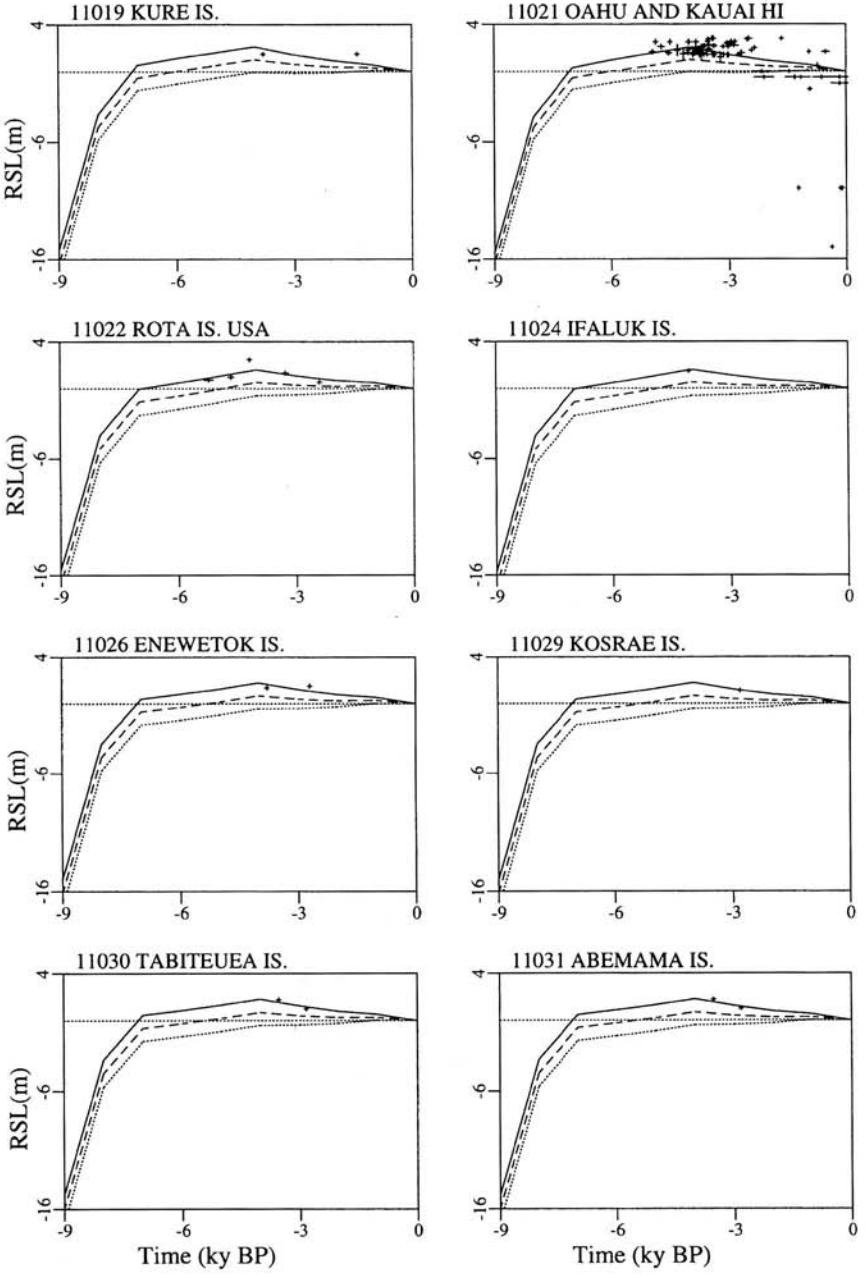

Figure 4.11 Comparisons of the predictions of the version of the gravitationally self-consistent theory of postglacial relative sea level history that neglects rotational feedback with the observations of many of the island locations shown in Fig. 4.10. All three of the time series shown at each site have been computed using the VM2 viscosity model but differ from one another in that they correspond to three variations on the ICE-4G deglaciation history. In particular the solid lines are the RSL predictions delivered by ICE-4G itself, the dotted lines are for a deglaciation

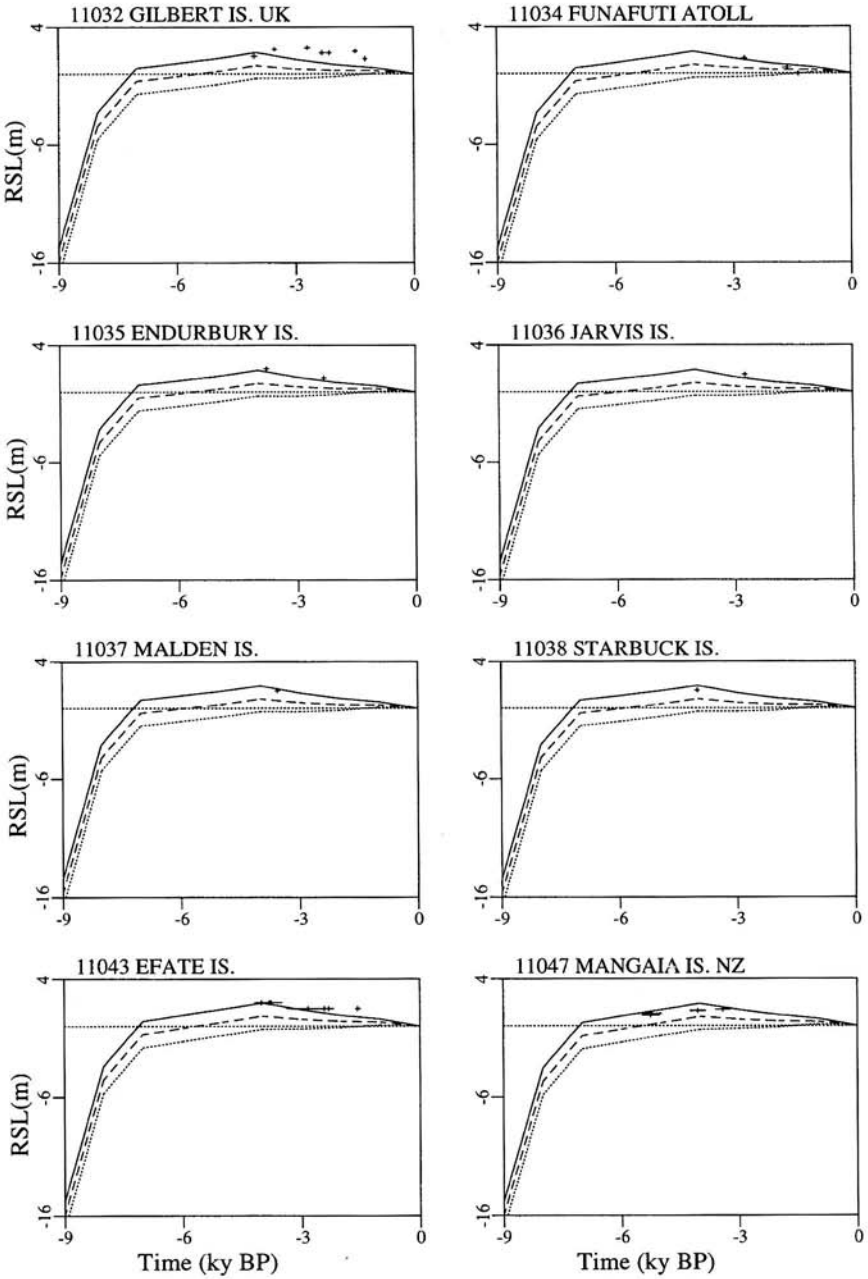

history that is identical to ICE-4G from LGM until 4 kyr BP, following which it is assumed that Antarctic melting continues to deliver water to the global ocean at an eustatic rate of 0.25 mm/yr. The dashed RSL curves are for a model that is identical to that which produces the dotted RSL curves but for which the post–4-kyr BP "melting tail" is of strength 0.5 mm/yr. It will be noted that neither of the models that include late Holocene melting from Antarctica is able to fit any of the data.

that continuing late Holocene melting of the polar ice caps on Greenland and Antarctica might be contributing significantly to the tide gauge inferred modern rate of global sea level rise of 1.8 mm/yr, is untenable. They suggest that as much as 0.5 mm/yr of this signal could be due to such continuing polar ice sheet instability. Clearly this rate, or any significant fraction of it, would rule out the existence of the mid-Holocene highstand of sea level that is observed at both Pacific island locations and at virtually all coastal locations in the far field of the ice sheets (results not shown).

Since it is the existence of the GIA-related mid-Holocene highstand of sea level and the subsequent fall to modern levels that leads to the increase in the tide gauge rates of relative sea level rise at far field sites when the tide gauge rate is corrected for the influence of glacial isostatic adjustment (see the results for individual gauges shown in Table 4.1), we may also usefully express the impact of the late Holocene melting postulated by Flemming *et al.* (1998) in the form of global maps of the predicted present-day rate of RSL rise due to the GIA process. Figure 4.12 (see color plate) provides a useful demonstration of the utility of a presentation of this kind. The top of this figure shows the predicted present-day rate of RSL rise for the standard ICE-4G (VM2) model, whereas the middle and bottom respectively show equivalent predictions for the models that incorporate the influence of Antarctica derived "melting tails" of global strength 0.25 and 0.50 mm/yr. Clearly, when the strength of late Holocene melting is taken to be the larger value, the sign of the present-day rate of GIA-related RSL rise in the far field is no longer negative but is positive, as the highstand has been entirely eliminated.

On the basis of these analyses of the implications of the observed mid-Holocene highstand of sea level at sites distant from the polar ice sheets, it should be clear that the existence of this ubiquitous feature places strong constraints upon the extent to which these ice sheets may have continued to supply meltwater to the sea from mid-Holocene time onward. Based upon the analysis of these data discussed herein, I would therefore suggest that an upper bound on the rate of sustained mass loss from these systems should be taken to be no more than 0.1 mm/yr. This is clearly an insignificant fraction of the global rate of sea level rise of 1.8 mm/yr that we are required to explain. If the polar ice sheets are making a significant contribution to this global rate, then this contribution must have been activated only recently and could therefore plausibly be related to modern climate change. Even if we consider such contributions to be of relatively recent vintage, however, their magnitude is still rather strongly constrained by other geophysical observations. In particular, it has been demonstrated in Peltier (1998a, 1999) that Earth rotation observations of the nontidal acceleration of the rate of axial rotation and the speed and direction of true polar wander strongly constrain the present-day rate of mass loss from these polar locations. These analyses suggest that the maximum rate of collective mass loss from Greenland and Antarctica that could be accommodated by these observations is 0.5 mm/yr and this would

be possible only under very special circumstances. In particular, Greenland would have to be the primary source of melting and the contributions from GIA and from the melting of small ice sheets and glaciers (e.g., Meier, 1984) would have to be most accommodating. If these constraints on the RSL contributions from the large polar ice sheets are correct, then we are clearly obliged to look elsewhere for explanation of the 1.8 mm/yr global sea level rise signal that the GIA-corrected tide gauge data reveal.

4.6 SUMMARY

A very detailed global viscoelastic theory of the process of glacial isostatic adjustment (GIA) has been developed. Application of this theory to the prediction of postglacial relative sea level histories has demonstrated that most ^{14}C-dated observations, from all sites in the global data base, are well explained by a spherically symmetric viscoelastic model whose elastic structure is fixed to that of PREM and whose radial viscosity profile is that of the VM2 model. Of course, there are exceptions to this general rule concerning the goodness of fit of the predictions of the spherically symmetric model to the observations. For example, at locations such as the Huon Peninsula of Papua New Guinea, where the entire coastline is being uplifted coseismically, the predictions of the GIA model fail to explain the observations (see Peltier, 1998a,d). It is expected that at other tectonically active locations similar misfits of the spherically symmetric theory to the observations should also be evident. Examples of such regions would certainly include the Mediterranean Sea region, Japan, and perhaps also the Pacific Northwest of North America where the Cordilleran ice sheet played a strong role in controlling the local history of relative sea level change but which is also influenced by active subduction.

These regions of misfit to the RSL predictions of the global viscoelastic theory of postglacial sea level change not withstanding, the extent to which this global spherically symmetric theory has been successful in reconciling the vast majority of the observations is satisfying, especially because only a very small subset of the observations has been employed to tune the model's radial profile of mantle viscosity. As discussed in greater detail in Peltier (1998b), these observations consisted of the set of wavenumber-dependent relaxation times determined by McConnell (1968) as characterizing the relaxation of Fennosandia following removal of its LGM ice load (the validity of which has recently be reconfirmed by Wieczerkowski *et al.,* 1999, as previously mentioned), a set of 23 site-specific relaxation times from locations in both Canada and Fennoscandia, and the observed nontidal rate of the acceleration of axial rotation. The VM2 viscosity model that was determined on the basis solely of these data, using the formal procedure of Bayesian inference with the simple four-layer VM1 model as a starting model, was thereafter (Peltier

1996) shown to immediately reconcile the dramatic misfits of the starting model to the high-quality data set of ^{14}C-dated RSL histories that is available from the east coast of the continental United States (see also Peltier, 1998a). Because these data were not employed to constrain the radial viscosity structure, this is an extremely meaningful test of the validity of the model. That the new model also very well reconciles relative sea level data from far field sites throughout the equatorial Pacific Ocean has also been demonstrated explicitly in this chapter (see Figs. 4.9 and 4.10). The observations from the latter region offer a means by which we may strongly constrain the rate of mass loss from the great polar ice sheets on Antarctica and Greenland that may have been occurring continuously since mid-Holocene time. Our analysis demonstrates that the extent to which this influence could be contributing to the present-day observed rate of global sea level rise is negligibly small, a conclusion that is inconsistent with the claim to the contrary by Flemming *et al.* (1998).

Application of the global theory of the glacial isostatic adjustment process to filter this influence from the tide gauge data is clearly justified by the high-quality fits that the model delivers to the (widely distributed in space) observations of RSL variability on geological timescales over which ^{14}C dating may be employed to accurately determining sample age. As demonstrated through the analyses summarized in Tables 4.1 and 4.2, application of the GIA filter sharply reduces the standard deviation of the individual tide gauge measurements of the rate of RSL rise from their mean value, demonstrating the importance of this step in the analysis procedure. As demonstrated in Table 4.2, application of the filter to an aggregated set of tide gauge data, in which sites are lumped together if they are close in geographical location, also leads to an increase in the estimated global rate of RSL rise. In either case (Table 4.1 or Table 4.2) the best estimate we have been able to produce of the global rate of RSL rise that could be related to ongoing climate change in the Earth system is between 1.91 and 1.84 mm/yr.

An important additional result that follows from the results listed in Table 4.1 concerns the comparison between the GIA-corrected rates of RSL rise on tide gauges located along the east coast of the continental United States that would be obtained by least-squares fitting a straight line to the geological data over a period of 3–4 kyr and the result that is obtained by using the geological rate that obtains over the same time period over which RSL is sampled by the tide gauges. This has been investigated by using the GIA-predicted rates as proxy for the actual geological data and computing the GIA-corrected rates listed in the column labeled LSQ in Table 4.1. Comparing the results in this column with the average of those in the -0.5 and $+0.5$ kyr columns for all U.S. east coast sites will show that the procedure of least-squares fitting a straight line to the geological data over a period of 3–4 kyr will significantly overestimate the magnitude of the GIA-related signal and therefore its use will lead to a significant underestimate of the filtered tide gauge result. This fact very directly explains the reason for the approximately

0.4 mm/yr difference between the GIA-corrected rates for the U.S. east coast determined by Peltier (1996b) and those previously determined by Gornitz (1995), the former result being near 1.9 mm/yr and the latter near 1.5 mm/yr.

In concluding discussion of the analyses presented in this chapter, it is useful to reflect upon their implications concerning the relative importance of the various sources that might be contributing to the inferred global rate of relative sea level rise whose magnitude has been herein implied to be somewhat in excess of 1.8 mm/yr (between 1.91 and 1.84 mm/yr). The most recent estimates of the contribution from small ice sheets and glaciers (Meier and Bahr, 1996) are that this source has a strength of 0.3 ± 0.1 mm/yr. The influence of permafrost melting is expected to be even smaller with a strength of 0.1 ± 0.1 mm/yr. I have argued herein that the contribution due to continuing late Holocene melting of polar ice from either Antarctica or Greenland is bounded above by 0.1 mm/yr. Since the most recent estimate of the terrestrial storage term (Chapter 5) suggests this to be -0.9 ± 0.5 mm/yr (note that this is revised from the previous estimate of -0.3 ± 0.15 mm/yr obtained by Gornitz *et al.* 1997) there is clearly a residual that requires explanation in terms of significant contributions from either Greenland and/or Antarctica and/or from the thermal expansion of the oceans. Since the geophysical constraint through Earth rotation observations (Peltier 1998a, 1999) appears to require the former to be less than 0.5 mm/yr, the implication of these arguments would appear to be that the current rate of global sea level rise due to thermal expansion of the oceans might be significantly larger than the rate usually assumed to best represent this contribution (0.6 ± 0.2 mm/yr). In connection with the latter contribution, however, it is not at all clear that the current generation of coupled atmosphere–ocean models, the results from which provide a primary basis for this estimate, are capable of accurately gauging the significance of this steric effect. Clearly much further effort, especially in strengthening the observational constraint on the steric signal and in more precisely estimating the contribution due to terrestrial storage will be required before we shall be in any position to be confident as to which of these conventionally considered influences is more important. If terrestrial storage were entirely unimportant, then the observed present day rate of rsl rise would be within the upper bound defined by the net influence of the other contributions. However, if the (negative) influence of terrestrial storage is as large as the most recent estimate (see Chapter 5), then the influence of thermal expansion (or one of the other contributions) would have to be considerably larger than the above stated estimates in order that the inferred global rate of rsl rise be successfully explained.

REFERENCES

Bills, G. B. and James, T. S. (1996). Late Quaternary variations in relative sea level due to glacial cycle polar wander. *Geophys. Res. Lett.* **23,** 3023–3026.

Cathles, L. M. (1975). *The Viscosity of the Earth's Mantle.* Princeton Univ. Press, Princeton, NJ.

Clark, J. A., Farrell, W. E., and Peltier, W. R. (1978). Global changes in postglacial sea level: A numerical calculation. *Quat. Res.* **9,** 265–287.

Dahlen, F. A. (1976). The passive influence of the oceans upon the rotation of the Earth. *Geophys. J. R. Astron. Soc.* **46,** 363–406.

Douglas, B. D. (1991). Global sea level rise. *J. Geophys. Res.* **96,** 6981–6992.

Dziewonski, A. M. and Anderson, D. L. (1981). Preliminary reference Earth model. *Phys. Earth Planet. Inter.* **25,** 297–356.

Farrell, W. E. (1972). Deformation of the Earth by surface loads. *Rev. Geophys.* **10,** 761–797.

Farrell, W. E. and Clarke, J. A. (1976). On postglacial sea level. *Geophys. J. R. Astron. Soc.* **46,** 647–667.

Fleming, K., Johnston, P., Zwartz, D., Yokoyama, Y., Lambeck, K., and Chappell, J. (1998). Refining the eustatic sea level curve since the Last Glacial Maximum using far-intermediate-field sites. *Earth Planet. Sci. Lett.* **163,** 327–342.

Gornitz, V. (1995). A comparison of differences between recent and late Holocene sea-level trends from eastern North America and other selected regions. *J. Coastal Res.* **17,** 287–297.

Gornitz, V., Rosenzweig, C., and Hillel, D. (1997). Effects of anthropogenic intervention in the land hydrological cycle on global sea level rise. *Global and Planetary Change* **14,** 147–161.

Grossman, E. E., Fletcher, C. H., III, and Richmond, B. M. (1998). The Holocene sea-level high stand in the equatorial Pacific: Analysis of the insular paleosea-level data base. *Coral Reefs* **17,** 309–327.

McConnell, R. K. (1968). Viscosity of the mantle from relaxation time spectra of isostatic adjustment. *J. Geophys. Res.* **73,** 7089–7105.

Meier, M. (1984). Contribution of small glaciers to global sea level. *Science* **226,** 1418–1421.

Meier, M. F. and Bahr, D. B. Counting glaciers: Use of scaling methods to estimate the number and size distribution of the glaciers of the world. In Colbeck, S. C. (ed.), *Glaciers, Ice Sheets and Volcanoes: A Tribute to Mark F. Meier.* CRREL Special Report 96-27, 89-94. U.S. Army, Hanover, NH.

Mitrovica, J. X., and Peltier, W. R. (1991). On postglacial geoid subsidence over the equatorial oceans. *J. Geophys. Res.* **96,** 20053–20071.

Mitrovica, J. X. and Forte, A. M. (1997). Radial profile of mantle viscosity: Results from the joint inversion of convection and postglacial rebound observables. *Geophys. J. Int.* **102,** 2751–2769. 1997.

Munk, W. H. and MacDonald, G. F. (1960). *The Rotation of the Earth.* Cambridge Univ. Press, New York, 1960.

Peltier, W. R. (1974). The impulse response of a Maxwell Earth. *Rev. Geophys.* **12,** 649–669.

Peltier, W. R. (1976). Glacial isostatic adjustment II: The inverse problem. *Geophys. J. R. Astron. Soc.* **46,** 669–706.

Peltier, W. R. (1982). Dynamics of the ice-age Earth. *Adv. Geophys.* **24,** 1–146.

Peltier, W. R. (1985). The LAGEOS constraint on deep mantle viscosity: Results from a new normal mode method for the inversion of viscoelastic relaxation spectra. *J. Geophys. Res.* **90,** 9411–9421.

Peltier, W. R. (1994). Ice-age paleotopography. *Science* **265,** 195–201.

Peltier, W. R. (1996a). Mantle viscosity and ice-age ice-sheet topography. *Science* **273,** 1359–1364.

Peltier, W. R. (1996b). Global sea level rise and glacial isostatic adjustment: An analysis of data from the east coast of North America. *Geophys. Res. Lett.* **23,** 717–720.

Peltier, W. R. (1998a). Postglacial variations in the level of the sea: Implications for climate dynamics and solid earth geophysics. *Rev. Geophys.* **36,** 603–689.

Peltier, W. R. (1998b). The inverse problem for mantle viscosity. *Inverse Problems* **14,** 441–478.

Peltier, W. R. (1998c). "Implicit Ice" in the global theory of glacial isostatic adjustment. *Geophys. Res. Lett.* **25,** 3957–3960.

Peltier, W. R. (1998d). Glacial isostatic adjustment and coastal tectonics. In *Coastal Tectonics,* Special Publication No. 146, Geological Society of London, 1–30.

Peltier, W. R. (1999). Global sea level rise and glacial isostatic adjustment. *Global and Planetary Change* **20,** 93–123.

Peltier, W. R., and Andrews, J. T. (1976). Glacial isostatic adjustment. I. The forward problem. *Geophys. J. R. Astron. Soc.* **46,** 605–646.

Peltier, W. R., Farrell, W. E., and Clark, J. A. (1978). Glacial isostasy and relative sea level: A global finite element model. *Tectonophysics* **50,** 81–110.

Peltier, W. R., and Tushingham, A. M. (1989). Global sea level rise and the greenhouse effect: Might they be connected? *Science* **244,** 806–810.

Shackleton, N. J., Berger, A., and Peltier, W. R. (1990). An alternative astronomical calibration of the lower Pleistocene timescale based upon ODP site 677. *Trans. R. Soc. Edinburgh Earth Sci.* **81,** 251–261.

Wieczerkowski, Karin, Mitrovica, Jerry X., and Wolf, Detlef. (1999). A revised relaxation-time spectrum for Fennoscandia. *Geophys. J. Int.* **139,** 69–86, 1999.

Wu, P. and Peltier, W. R. (1984). Pleistocene deglaciation and the Earth's rotation: A new analysis. *Geophys. J. R. Astron. Soc.* **76,** 202–242.